Chemically and electrically tunable spin polarization in ferroelectric Cd-based hybrid organic-inorganic perovskites

Ravi Kashikar,[1,*] P. S. Ghosh,[1,2] S. Lisenkov,[1] B. R. K. Nanda,[3,4] and I. Ponomareva[1,†]
[1]*Department of Physics, University of South Florida, Tampa, Florida 33620, USA*
[2]*Glass & Advanced Materials Division, Bhabha Atomic Research Centre, Mumbai 400 085, India*
[3]*Condensed Matter Theory and Computational Lab, Department of Physics, Indian Institute of Technology Madras, Chennai 600036, India*
[4]*Center for Atomistic Modelling and Materials Design, Indian Institute of Technology Madras, Chennai 600036, India*

(Received 10 September 2021; revised 31 October 2021; accepted 2 December 2021; published 17 December 2021)

Density functional theory computations are used to predict the electronic structure of Cd-based hybrid organic-inorganic high-T_C ferroelectric perovskites with TMCM-$CdCl_3$ being one representative. We report Rashba-Dresselhaus spin splitting in the valence band of these nonmagnetic compounds. Interestingly, we find in computations that the splitting is not necessarily sensitive to the polarization of the material but to the organic molecule itself which opens a way to its chemical tunability through the choice of the molecule. Further chemical tunability of spin splitting is shown to be possible through a substitution of Cl in the $CdCl_3$ chains as the valence band was found to originate from Cl-Cl weekly bonding orbitals. For example, the substitution of Cl with Br in TMCM-$CdCl_3$ resulted in a ten times increase of spin splitting. Furthermore, the spin polarization in these materials gives origin to persistent spin textures which are coupled to the polarization direction, and, therefore, can be controlled by the electric field. This is promising for spintronics applications.

DOI: 10.1103/PhysRevB.104.235132

I. INTRODUCTION

Ferroelectrics are the materials that exhibit spontaneous polarization in the absence of the electric field. They find numerous applications in dynamic random access memories, transduction sensors and actuators [1,2]. Recently, cofunctionality between ferroelectricity and Rahsba spin splitting has been established in GeTe [3–6] and predicted in several ferroelectrics [7–13]. Such cofunctionality is understood as the coexistence of ferroelectricity and spin polarization in the same material and typically implies the possibility to control the latter by the direction and/or magnitude of ferroelectric polarization. For example, reversal of polarization by the electric field has been shown to result in the reversal of the spin-texture direction [7,14]. Such cofunctionality is very attractive for nonvolatile spintronic devices [14]. However, so far it has been explored mostly in inorganic ferrorlectrics.

Hybrid organic inorganic ferroelectrics/piezoelectrics are recently emerging as an attractive alternative to the traditional inorganic ones as they feature several advantages: lack of toxic elements, flexibility, low synthesis temperature, and larger chemical tunablity [15–18]. Can these materials also exhibit the aforementioned spin polarization/ferroelectricity cofunctionality? Very limited insights are available at the moment. Switchable Rashba bands have been predicted for the basic halide perovskite ferroelectrics family [19]. More recently, Lou *et al.* [20] used density functional theory (DFT) calculations to predict Rashba-like band splitting and persistent spin textures in antiferromagnetic hybrid organic inorganic perovskite (HOIP) TMCM-$MnCl_3$ (TMCM=trimethylchloromethyl ammonium). Remarkably, the spin textures were found to be tunable by switching the magnetic ordering or ferroelectric polarization. The family of TMCM-$MnCl_3$, TMCM-$CdCl_3$, and $TMC_{1-x}F_xM$-$CdCl_3$ materials is very attractive as they exhibit high Curie temperature, large piezoelectric response [15,17], which was predicted to originate from phase switching [21], and property tunability by pressure [22]. This impressive diversity of cofunctionalities suggests further investigation into the possibility to observe electrically tunable spin polarizations and spin-textures in its nonmagnetic members, TMCM-$CdCl_3$ and $TMC_{1-x}F_xM$-$CdCl_3$, which, to the best of our knowledge, has not been reported this far. Furthermore, it is presently unknown whether the spin polarizations in cofunctional hybrid ferroelectrics are chemically tunable. Motivated to fill up this gap in understanding of nonmagnetic Cd-based HOIP, we aim: (i) to predict that they exhibit band splitting, spin polarizations, and electrically tunable spin textures; (ii) to predict chemical tunability of these properties and its atomistic origin; and (iii) to reveal the nontrivial role that the organic molecule plays in the effect. The rest of the paper is organized as follows: in Sec. II, we present computational details; in Sec. III, we focus on changes in the band structure of perovskite due to large structural disotortions associated with the formation of HOIP structure; in Sec. IV, we present spin splitting and spin polarization in Cd-based HOIP; and in Sec. V, we predict their chemical and electrical tunability. In Sec. VI, we summarize the work.

II. COMPUTATIONAL DETAILS

DFT-based pseudopotential methodology with Perdew-Burke-Ernzerhof (PBE) exchange-correlation functional [23]

*ravik@usf.edu
†iponomar@usf.edu

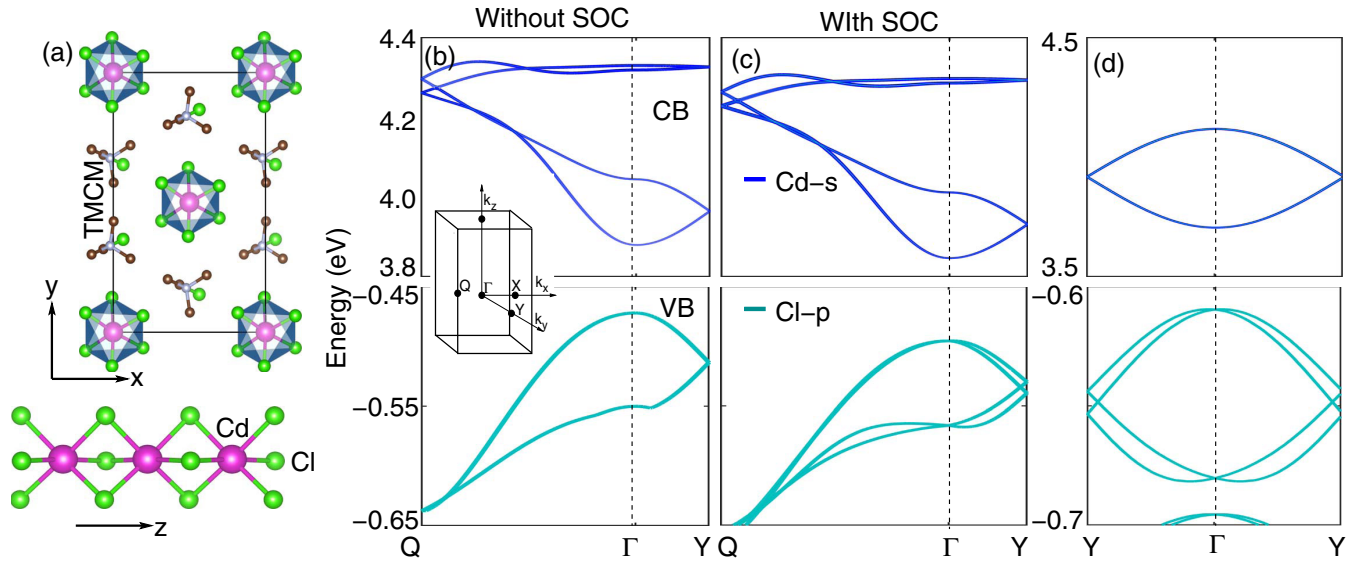

FIG. 1. (a) Conventional cell of TMCM-$CdCl_3$ and chain of $CdCl_6$ octahedra. TMCM molecules in the unit cell are presented without hydrogen atoms. Orbital resolved band structure of TMCM-$CdCl_3$ in absence (b) and presence (c) of SOC. Band structure along Y-Γ-Y path, where the spin splitting is maximum (d). The inset in (b) shows the Brillouin zone.

as implemented in Vienna *ab initio* simulation package (VASP) [24] was utilized for this study. The electron-ion interactions are treated with the projected augmented wave (PAW) potentials [25]. Zero damping D3 dispersion corrections as proposed by Grimme *et al.* [26] are incorporated in the simulations. A cutoff energy of 700 eV for the plane wave basis set is used and a $4 \times 2 \times 4$ Monkhorst-Pack k-point mesh is employed for the integration over the Brillouin zone. This choice ensures energy convergence of 0.002 eV/f.u. All structural relaxations are carried out using conjugate gradient algorithm until ionic forces are less than 2 meV/Å, which results in residual stresses less than 0.05 GPa. All the electronic structure calculations are carried out with spin-orbit coupling (SOC), unless specified. The polarization is computed using modern theory of polarization developed by King-Smith and Vanderbilt [27].

III. BAND STRUCTURE OF HIGHLY DISTORTED PEROVSKITE

Let us begin by inspection of TMCM-$CdCl_3$ structure given in Fig. 1(a) and notice that it is rather different from the prototypical perovskite ABX_3. Therefore it is imperative to understand what structural transformations relate this structure to prototypical perovskite ABX_3 and what effect they may have on its electronic structure. To address this question, we look into two inorganic counterparts of TMCM-$CdCl_3$: cubic $CsCdCl_3$ [shown in Fig. 2(a)] and a hypothetical monoclinic $CsCdCl_3$ [see Fig. 2(b)] that has the same space group as the TMCM-$CdCl_3$ ground state. The fully relaxed cubic $CsCdCl_3$ has the lattice parameter 5.32 Å, which agrees well with the experimental value 5.22 Å [28,29]. The crystal structure and the orbital resolved band structure of cubic $CsCdCl_3$ are shown in Fig. 2. The following observations can be made from the band structure: (i) The band structure around the Fermi level (E_F) is dominated by Cd-$\{s, p\}$ and Cl-p valence orbitals, which undergo covalent hybridization to create highly dispersive antibonding and bonding bands lying higher and lower in energy respectively with a set of weakly dispersive bands in the middle [30]. With 18 valence electrons per

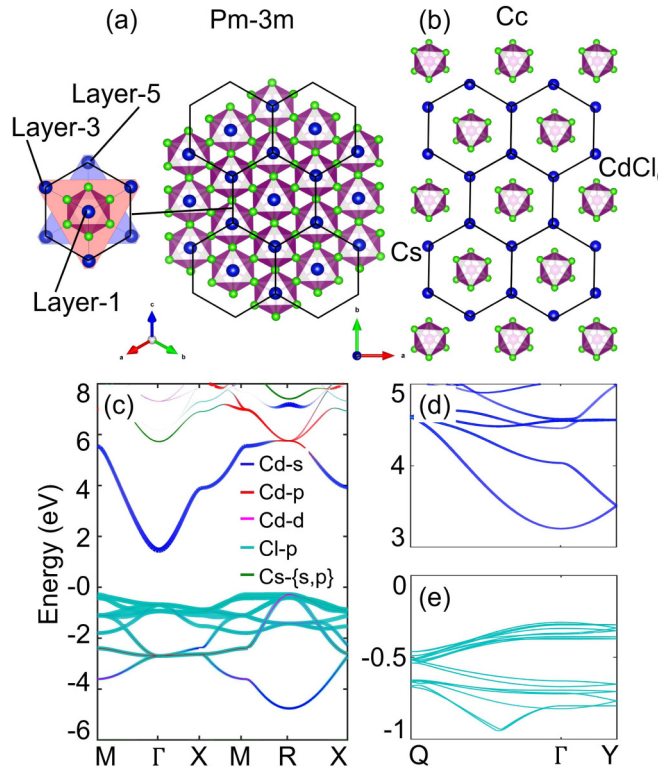

FIG. 2. Top view of the crystal structure of $CsCdCl_3$ in cubic phase projected along [111] (a) and in a hypothetical monoclinic phase resembling that of the TMCM-$CdCl_3$ (b). The $CdCl_6$ octahedra complexes are shown. Orbital resolved band structure of the cubic (c) and monoclinic [(d) and (e)] $CsCdCl_3$.

unit cell, the E_F lies between Cl-p dominated weakly bonding and Cd-s dominated antibonding states. The conduction band minimum and valence band maximum are formed at Γ and R respectively to create an indirect band gap of 1.7 eV. The cubic to monoclinic structural transformation can be understood from the projection of the cubic perovskites along the [111] direction as shown in Fig. 2(a). The alternate stacking of Cs and Cd layers gives rise to a triangular-hexagonal pattern. In the monoclinic phase, as shown in Fig. 2(b), the redistribution of Cs and Cd occurs where the columns of Cd lying at the center of each hexagon formed by the Cs atoms. Such a transformation distorts the octahedra significantly and isolate them in the ab plane, while a chain of them is formed along the c axis. The lack of axial Cd-Cl-Cd covalent bonding involving the p orbitals, both due to isolation and distortion, resulted in the formation of narrow bands as reflected in Figs. 2(d) and 2(e). We estimated the band width of a valence band in the monoclinic phase to be in the range 0–0.2 eV, whereas in the cubic phase, it can be as large as 3 eV.

IV. SPIN SPLITTING AND SPIN POLARIZATIONS IN CD-BASED HOIP

Having achieved the basic understanding of the role structural distortion play in the electronic structure of the inorganic counterparts we turn to TMCM-$CdCl_3$. The calculations were carried out on the fully relaxed TMCM-$CdCl_3$ structure (Cc space group), whose parameters are the ones previously reported by us in Ref. [21] and agree well with experimental values at 293 K [17]. They are 9.3 Å, 15.5 Å, 6.9 Å, and $\beta = 94.6^\circ$. We direct x, y, and z axes along a, b and c crystallographic directions, respectively. The structure is shown in Fig. 1(a), whose local environment and orbital interactions resemblance to the inorganic $CsCdCl_3$. The orbital resolved band structure computed without incorporation of SOC is presented in Fig. 1(b). The lowest conduction band is of Cd-s (∼65%) and Cl-p (∼35%) orbital characters with minimum at the Γ point. This is in contrast with the Cd-s dominated orbital character of the cubic $CsCdCl_3$ conduction band and is attributed to the distortion of the octahedral cage. The valence band spectrum is of the predominantly Cl-p orbital character and small fraction of Cd-d orbital character with the maximum at Γ point. The valence band spectrum is less dispersive as compared to the conduction band spectrum due to the weakly bonded nature of Cl-p orbitals. The calculations predict a direct band gap of 4.35 eV which could be compared with experimental value of 5.51 eV [31]. The band gap is enhanced with respect to cubic $CsCdCl_3$ due to the aforementioned octahedral isolations and large-scale distortions that decrease the orbital overlap strength. It should be noted that further improvement in the band gap prediction can be achieved by using hybrid functionals. However, due to their computational cost, they have not been applied for this study. Furthermore, in case of inorganic ferroelectric perovskites, it was found that nonhybrid functionals outperform the hybrid ones for ferroelectricity-related properties [32]. Figure 1(c) shows the orbital resolved spin-orbit coupled band structure. The notable feature is spin splitting in the valence bands away from high-symmetry k points (Q, Γ, and Y). It should be noted that we find negligibly small spin splitting in the conduction band also. The Cc space group of TMCM-$CdCl_3$ is noncentrosymmetric and, therefore, could exhibit spin polarizations (Rashba and/or Dresselhaus type) [10]. Figure 3 gives the two highest energy valence bands and their two dimensional cross sections. We find spin splitting along the k_x and k_y directions, but no splitting along the k_z direction. To gain further understanding and quantify spin splitting, we develop an effective Hamiltonian for the structure. TMCM-$CdCl_3$ belongs to C_s point group symmetry, which has a mirror plane M_y [see Fig. 1(a)]. Table I lists symmetry invariants under all relevant symmetry operations as reported in Ref. [14].

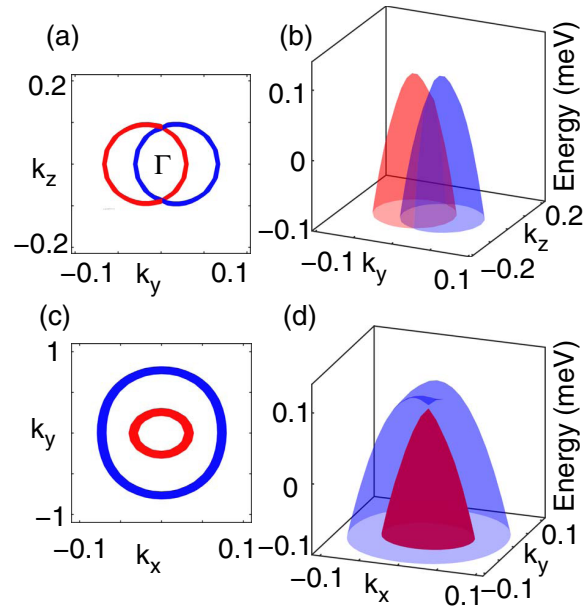

FIG. 3. Two-dimensional cross-section of valence bands for the 5-meV ranges in different planes (a) and (c) and the corresponding three-dimensional plots (b) and (d). The two bands shown in red and blue corresponds to the spin-up and spin-down channels; k_x, k_y, and k_z are multiple of $2\pi/a$, $2\pi/b$, and $2\pi/c$, respectively and in units of $Å^{-1}$.

The effective Hamiltonian is constructed by retaining common invariants from all the symmetry operations and is

$$H = \frac{\hbar^2}{2}\left(\frac{k_x^2}{m_x} + \frac{k_y^2}{m_y} + \frac{k_z^2}{m_z}\right) + \alpha k_x \sigma_y + k_y(\beta\sigma_x + \gamma\sigma_z) + k_z\delta\sigma_y, \quad (1)$$

where α, β, γ, and δ are the adjustable parameters which can be obtained from fitting the eigenvalues of the Hamiltonian to

TABLE I. Symmetry operators and corresponding invariants for C_s point group symmetry.

Symmetry	(k_x, k_y, k_z)	$(\sigma_x, \sigma_y, \sigma_z)$	Invariants
$T = i\sigma_y K$	$(-k_x, -k_y, -k_z)$	$(-\sigma_x, -\sigma_y, -\sigma_z)$	$k_x\sigma_x, k_x\sigma_y, k_x\sigma_z$ $k_y\sigma_x, k_y\sigma_y, k_y\sigma_z$ $k_z\sigma_x, k_z\sigma_y, k_z\sigma_z$
$M_y = i\sigma_y$	$(k_x, -k_y, k_z)$	$(-\sigma_x, \sigma_y, -\sigma_z)$	$k_x\sigma_y, k_z\sigma_y$ $k_y\sigma_x, k_y\sigma_z$

TABLE II. Effective interaction (t_x, t_y, and t_z) and spin-splitting strengths (α–δ) in meV Å^{-2} and meV Å, respectively.

Compound	t_x	t_y	t_z	α	β	γ	δ
TMCM-$CdCl_3$	−3.7	−4.8	−26.0	1.0	0.0	1.6	0.1
TMBM-$CdBr_3$	−4.6	−10	−27.5	2.5	2.5	6	2.5
TMBM-$CdCl_3$	−5.3	−7.5	−25	2	0	2.5	1
TMCM-$CdBr_3$	−2.2	−6	−28	8	0	2.8	3
$CsCdCl_3$	−5	0.1	−19	0.3	0	0.6	0.1

the DFT computed ones. For example, for the k_y-k_z plane the matrix form of the Hamiltonian is

$$H = \begin{pmatrix} \frac{\hbar^2}{2}\left(\frac{k_y^2}{m_y} + \frac{k_z^2}{m_z}\right) + k_y\gamma & \beta k_y - i\delta k_z \\ \beta k_y + i\delta k_z & \frac{\hbar^2}{2}\left(\frac{k_y^2}{m_y} + \frac{k_z^2}{m_z}\right) - k_y\gamma \end{pmatrix}. \quad (2)$$

Technically, we fit the DFT band structure along directions Y-Γ-Y, X-Γ-X, and Z-Γ-Z separately. We numerically find the eigenvalues of the Hamiltonian for the given direction and adjust the fitting parameters until a good match with DFT predictions is achieved. Alternatively, we derived analytical expressions for the eigenvalues and eigenvectors of the Hamiltonian for different planes and used the former one to fit the DFT band structure. Both technical approaches yielded the same values of the adjustable parameters.

All the fitted parameters are listed in Table II, where we use $t_i = \frac{\hbar^2}{2m_i}[i = x, y, z]$ as the parameters that determine the curvature of the band. An analysis of the parameters strength indicates that the effective masses are k-dependent and have larger value along the k_x direction. In case of the TMCM-$CdCl_3$, we find that among the parameters that control spin splitting the largest values are for γ and α which explain the large splitting along the k_y and k_x directions.

The expectation value of spinors, $\sigma_i(i = x, y, z)$, give rise to a finite value of σ_z component which is proportional to spin splitting parameter γ. Other components σ_x and σ_y mainly depend on the β and δ, whose values are very small. Thus the TMCM-$CdCl_3$ exhibits persistent spin texture given in Fig. 4(a). In the case of k_x-k_y plane [Fig. 4(b)], the spin-texture as predicted by the effective Hamiltonian is of Dresselhauss type. However, due to a negligible strength of the β splitting parameter, σ_x is nearly zero and spin texture appears to be persistent in nature.

V. CHEMICAL AND ELECTRICAL TUNABILITY OF SPIN POLARIZATIONS

Next we set to understand the role that the TMCM molecule plays in the spin splitting. For that, we replace the molecule with Cs placed on the N site of TMCM. No structural relaxation is performed here as we are interested just in the contribution of the TMCM molecule. The calculated band structure of the $CsCdCl_3$ monoclinic conventional cell is shown in the Fig. 5(a). Interestingly, the splitting in the valence band has reduced to negligibly small values, despite the fact that the supercell exhibits spontaneous polarization of 3.5 μC/cm^2 that is comparable with the TMCM-$CdCl_3$ one. The finding suggests that it is the spatial charge distribution of

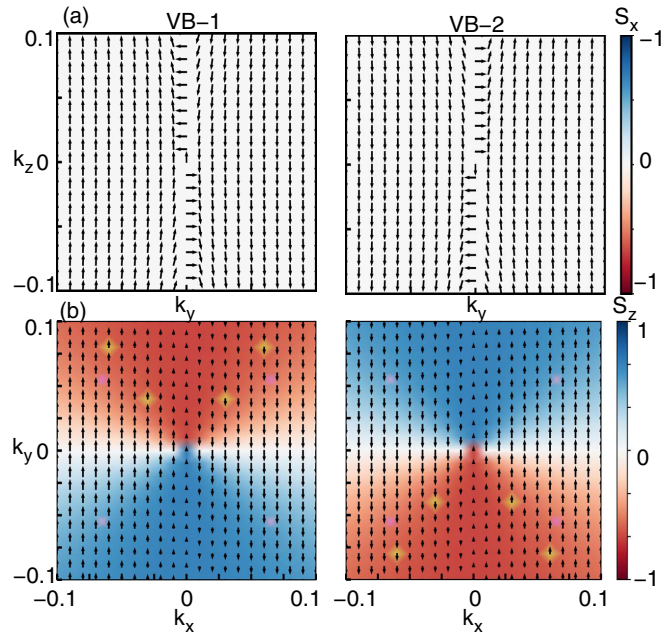

FIG. 4. Spin texture of valence bands of TMCM-$CdCl_3$ in the k_y-k_z (a) and k_x-k_y (b) planes, obtained from effective model Hamiltonian.

the organic molecule that is responsible for the spin splitting. Consequently, one may wonder whether the spin splitting is tunable by the organic molecule.

To answer this question, we extend our investigation to fluorine substituted $TMC_{1-x}F_xM$-$CdCl_3$ (TMCFM) ($x = 0.25$), which crystallize in the same Cc space group [17]. Technically, we replaced one TMCM molecule with a TMFM in the ground state structure of TMCM-$CdCl_3$ and carried out full structural relaxation. Both spin splitting and polarization, indeed, changed in this case, although rather slightly [see Fig. 5(b)]. The values are reported in Table III. As the next substitution, we replaced Cl by Br in the TMCM molecule and carried out full structural relaxation. In this case, we find larger change in the polarization with respect to TMCM-$CdCl_3$ and nearly 50% increase in the spin splitting [see Fig. 5(c) and Table III], which indeed confirm tunability of the spin splitting by the choice of the organic molecule and may open a way to property engineering.

TABLE III. Band-splitting computed at (0, 0.025, 0) point of the Brillouin zone and polarizations for various HOIPs.

Compound	Splitting Energy (meV)	Polarization (μC/cm^2)
TMCM-$CdCl_3$	0.11	(−3.3, 0, 4.5)
$TMC_{1-x}F_xM$-$CdCl_3$ ($x = 0.25$)	0.09	(−3.5, 0.0, 4.4)
TMBM-$CdCl_3$	0.15	(−2.5, 0, 4.6)
TMCM-$CdBr_3$	0.38	(−2.8, 0, 4.3)
TMBM-$CdBr_3$	0.91	(−2.3, 0, 4.3)
$CsCdCl_3$	0.00	(3.9, 0, −4.4)

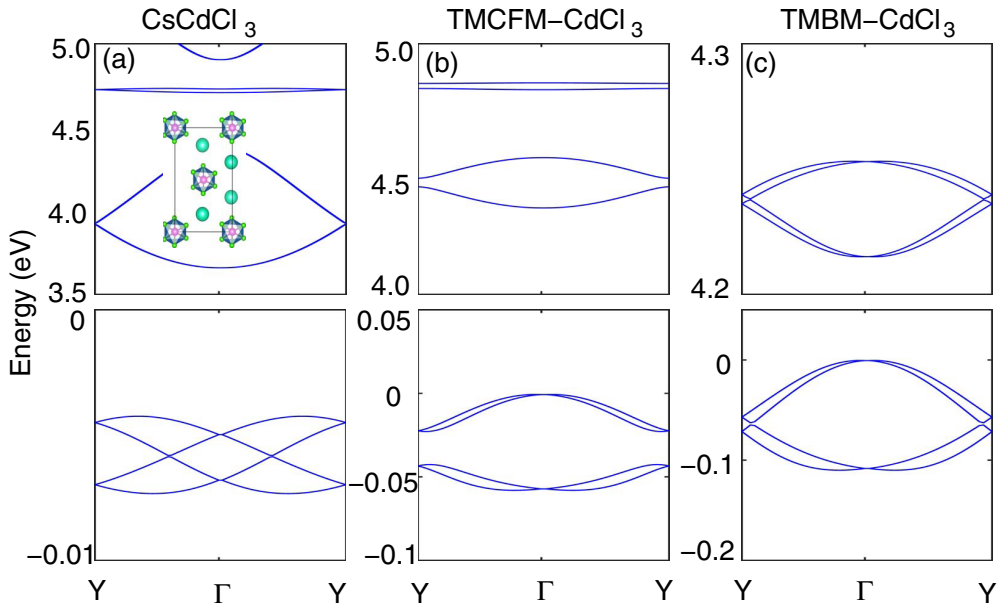

FIG. 5. Band structure of monoclinic $CsCdCl_3$ (a), $TMC_{1-x}F_xM$-$CdCl_3$ with $x = 0.25$ (b), and TMBM-$CdCl_3$ (c). Note the difference in the energy scale.

To further explore tunability of spin splitting in this family of compounds we recall that the conduction and valence band edges are dominated by B and X sites, respectively. We hypothesize that replacing Cl with Br on the X site will lead to enhancement of the spin splitting due to larger atomic SOC of Br. To test the hypothesis, we carried out band structure calculation for various combinations of Cl and Br atoms on organic molecule site and on X site of ABX_3, without altering the symmetry of the cell. We considered TMBM-$CdBr_3$ and TMCM-$CdBr_3$ in Cc space group. Among these compounds, TMCM-$CdBr_3$ is experimentally synthesized in space group $P6_3mc$ [33]. The computed band structure is presented in Fig. 6 and spin splittings and polarizations are listed in Table III. The data reveal that for TMBM-$CdBr_3$ and TMCM-$CdBr_3$ the spin splitting is enhanced by nine times and three times, respectively, as compared to TMCM-$CdCl_3$ band splitting. In addition, we now observe a small splitting in the conduction bands of TMBM-$CdBr_3$ and TMBM-$CdCl_3$. This is further illustrated in the strengths of the effective Hamiltonian coupling parameters in Table II. Br-based compounds have significantly larger values as compared to Cl, while $CsCdCl_3$ has the smallest splitting strength among all. We attribute these findings to the larger atomic number of Br compared to Cl, which enhances atomic SOC. One of the most attractive properties of the cofunctionality is the possibility to control spin polarizations by reversal of ferroelectric polarization. To test this in TMCM-$CdCl_3$, we inverted the ground state structure as suggested in Ref. [34] and repeated simulations. The polarization reversed its direction which resulted in the reversal of spin textures as shown in Fig. 7(b). This finding confirms the tunability of spin texture in this material by the electric polarization.

VI. SUMMARY

In summary, we have used DFT-based computations to investigate electronic structure of Cd-based HOIP and the effect that SOC has on it. We found that in the parent compound, cubic $CsCdCl_3$ conduction and valence band edges are dominated by Cd-s and Cl-p and originate from Cd-$\{s, p\}$-Cl-p molecular orbitals. This insight suggested the possibility to chemically tune the band edges through substitution on the X

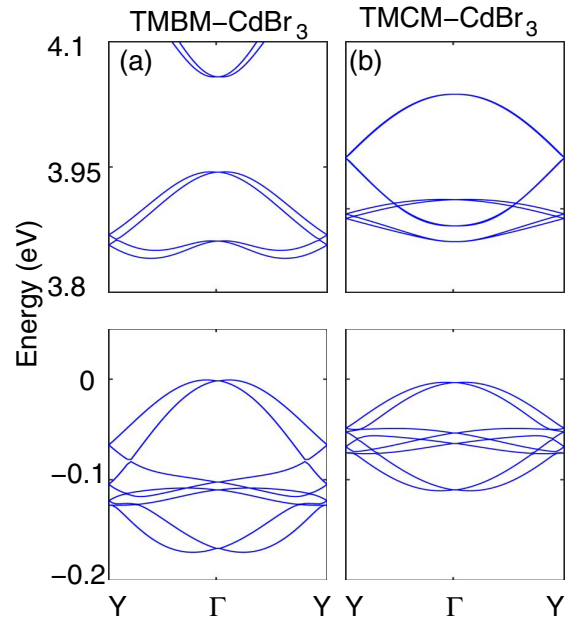

FIG. 6. Band structure of monoclinic TMBM-$CdBr_3$ (a) and TMCM-$CdBr_3$ (b).

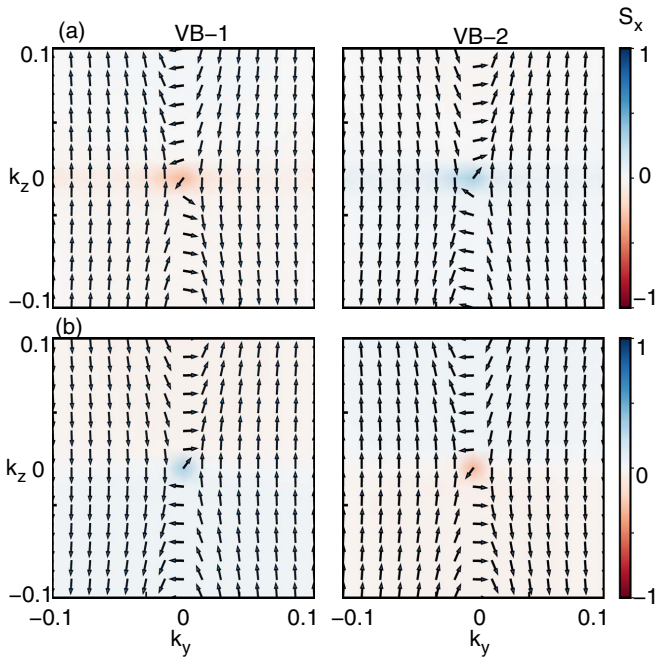

FIG. 7. Spin texture of valence bands of TMCM-$CdCl_3$ for the $10\bar{1}$ polarization (a) and for $\bar{1}01$ polarization (b) directions. The system exhibits the persistent spin texture oriented along the k_z direction and the direction is reversed for the opposite direction of polarization.

site. In the TMCM-$CdCl_3$ compound we found band splitting due to SOC. Such splitting is indeed allowed in this material as its structure lacks inversion symmetry. Interestingly, the spin splitting was found to correlate not as much with the material's polarization as with the spacial charge distribution introduced by the organic molecule. An effective Hamiltonian is proposed to gain insights into the band splitting and spin polarization. Interestingly, it predicts the Dresselhaus type of spin splitting in the *Cc* space group which, however, results in persistent spin textures in the materials studied due to the delicate interplay of the interaction strengths. From the practical perspective, the persistent spin textures are very attractive as they are found to be fully controllable by the polarization direction, which, in turn, can be manipulated by the electric field. Another finding that is also of practical significance is the high chemical tunability of the spin polarization. For example, replacing Cl with Br results in the ten times increase of the band splitting which we attribute to the higher atomic SOC of Br. Thus the study reveals both scientific and technological appeal of these emerging materials.

ACKNOWLEDGMENTS

This work is supported by the U.S. Department of Energy, Office of Basic Energy Sciences, Division of Materials Sciences and Engineering under Grant DE-SC0005245. B.R.K.N. acknowledges the support from Department of Science and Technology, India, through Grant No. CRG/2020/004330.

[1] J. F. Scott, Applications of modern ferroelectrics, Science **315**, 954 (2007).

[2] L. W. Martin and A. M. Rappe, Thin- film ferroelectric materials and their applications, Nat. Rev. Mater. **2**, 16087 (2016).

[3] J. Krempaský, S. Muff, J. Minár, N. Pilet, M. Fanciulli, A. P. Weber, E. B. Guedes, M. Caputo, E. Müller, V. V. Volobuev, M. Gmitra, C. A. F. Vaz, V. Scagnoli, G. Springholz, and J. H. Dil, Operando Imaging of All-Electric Spin Texture Manipulation in Ferroelectric and Multiferroic Rashba Semiconductors, Phys. Rev. X **8**, 021067 (2018).

[4] Q. Le-Van, X. Le Roux, A. Aassime, and A. Degiron, Electrically driven optical meta-materials, Nat. Commun. **7**, 12017 (2016).

[5] D. Di Sante, P. Barone, R. Bertacco, and S. Picozzi, Electric control of the giant rashba effect in bulk gete, Adv. Mater. **25**, 509 (2013).

[6] C. Rinaldi, S. Varotto, S. Asa, Picozzi, and R. Bertacco, Ferroelectric control of the spin texture in gete, Nano Lett. **18**, 2751 (2018).

[7] C. M. Acosta, A. Fazzio, G. M. Dalpian, and A. Zunger, Inverse design of compounds that have simultaneously ferroelectric and Rashba cofunctionality, Phys. Rev. B **102**, 144106 (2020).

[8] X. Zhang, Q. Liu, Jun Wei Luo, A. J. Freeman, and A. Zunger, Hidden spin polarization in inversion-symmetric bulk crystals, Nat. Phys. **10**, 387 (2014).

[9] L. D. Yuan, Z. Wang, J. W. Luo, E. I. Rashba, and A. Zunger, Giant momentum-dependent spin splitting in centrosymmetric low- Z antiferromagnets, Phys. Rev. B **102**, 014422(R) (2020).

[10] C. Mera Acosta, E. Ogoshi, A. Fazzio, G. M. Dalpian, and A. Zunger, The rashba scale: Emergence of band anti-crossing as a design principle for materials with large rashba coefficient, Matter **3**, 145 (2020).

[11] H. J. Zhao, P. Chen, C. Paillard, R. Arras, Y.-W. Fang, X. Li, J. Gosteau, Y. Yang, and L. Bellaiche, Large spin splittings due to the orbital degree of freedom and spin textures in a ferroelectric nitride perovskite, Phys. Rev. B **102**, 041203(R) (2020).

[12] J. Gosteau, R. Arras, P. Chen, H. J. Zhao, C. Paillard, and L. Bellaiche, Spin-orbit effects in ferroelectric $PbTio_3$ under tensile strain, Phys. Rev. B **103**, 024416 (2021).

[13] H. J. Zhao, H. Nakamura, R. Arras, C. Paillard, P. Chen, J. Gosteau, Xu Li, Y. Yang, and L. Bellaiche, Purely Cubic Spin Splittings with Persistent Spin Textures, Phys. Rev. Lett. **125**, 216405 (2020).

[14] L. L. Tao and E. Y. Tsymbal, Perspectives of spin-textured ferroelectrics, J. Phys. D **54**, 113001 (2021).

[15] Yu M. You, W. Q. Liao, D. Zhao, H. Y. Ye, Yi Zhang, Q. Zhou, X. Niu, J. Wang, Peng Fei Li, Da Wei Fu, Z. Wang, S. Gao, K. Yang, J. M. Liu, J. Li, Y. Yan, and R. G. Xiong, An organic-inorganic perovskite ferroelectric with large piezoelectric response, Science **357**, 306 (2017).

[16] W. Q. Liao, Y. Y. Tang, P. F. Li, Y. M. You, and R. G. Xiong, Large Piezoelectric Effect in a Lead-Free Molecular Ferroelectric Thin Film, J. Am. Chem. Soc. **139**, 18071 (2017).

[17] W. Q. Liao, D. Zhao, Yuan Yuan Tang, Yi Zhang, P. F. Li, P. P. Shi, X. G. Chen, Yu M. You, and R. G. Xiong, A molecular

perovskite solid solution with piezoelectricity stronger than lead zirconate titanate, Science **363**, 1206 (2019).

[18] D. Yang, L. Luo, Yi Gao, S. Chen, and X. C. Zeng, Rational design of one-dimensional hybrid organic-inorganic perovskites with room-temperature ferroelectricity and strong piezoelectricity, Materials Horizons **6**, 1463 (2019).

[19] M. Kim, J. Im, A. J. Freeman, J. Ihm, and H. Jin, Switchable s = 1/2 and j = 1/2 rashba bands in ferroelectric halide perovskites, Proc. Natl. Acad. Sci. USA **111**, 6900 (2014).

[20] F. Lou, T. Gu, J. Ji, J. Feng, H. Xiang, and A. Stroppa, Tunable spin textures in polar antiferromagnetic hybrid organic-inorganic perovskites by electric and magnetic fields, npj Comput. Mater. **6**, 1 (2020).

[21] P. S. Ghosh, S. Lisenkov, and I. Ponomareva, Phase Switching as the Origin of Large Piezoelectric Response in Organic-Inorganic Perovskites: A First-Principles Study, Phys. Rev. Lett. **125**, 207601 (2020).

[22] P. S. Ghosh, J. Doherty, S. Lisenkov, and I. Ponomareva, Tunability of structure, polarization, and band gap of high tc organic-inorganic ferroelectrics by hydrostatic pressure: First-principles study, J. Phys. Chem. C **125**, 16296 (2021).

[23] J. P. Perdew, K. Burke, and M. Ernzerhof, Generalized Gradient Approximation Made Simple, Phys. Rev. Lett. **77**, 3865 (1996).

[24] G. Kresse and J. Furthmüller, Efficient iterative schemes for ab initio total-energy calculations using a plane-wave basis set, Phys. Rev. B **54**, 11169 (1996).

[25] P. E. Blöchl, Projector augmented-wave method, Phys. Rev. B: Condens. Matter Mater. Phys. **50**, 17953 (1994).

[26] S. Grimme, Semiempirical GGA-type Density Functional Constructed with a Long range Dispersion Correction, J. Comput. Chem. **27**, 1787 (2006).

[27] R. D. King-Smith and David Vanderbilt, Theory of polarization of crystalline solids, Phys. Rev. B **47**, 1651(R) (1993).

[28] R. L. Moreira and A. Dias, Comment on prediction of lattice constant in cubic perovskites, J. Phys. Chem. Solids **68**, 1617 (2007).

[29] L.Q. Jiang, J.K. Guo, H.B. Liu, M. Zhu, X. Zhou, P. Wu, and C.H. Li, Prediction of lattice constant in cubic perovskites, J. Phys. Chem. Solids **67**, 1531 (2006).

[30] R. Kashikar, M. Gupta, and B. R. K. Nanda, A generic slater-koster description of the electronic structure of centrosymmetric halide perovskites, J. Chem. Phys. **154**, 104706 (2021).

[31] C. Ma, F. Chen, X. Song, M. Chen, L. Gao, P. Wang, J. Wen, Z. Yang, Centimeter-sized molecular perovskite crystal for efficient x-ray detection, Adv. Funct. Mater. **31**, 2100691 (2021).

[32] M. Kingsland, K. A. Lynch, S. Lisenkov, X. He, and I. Ponomareva, Comparative study of minnesota functionals performance on ferroelectric $BaTiO_3$ and $PbTiO_3$, Phys. Rev. Materials **4**, 073802 (2020).

[33] W.-Q. Liao, Y.-Y. Tang, P.-F. Li, Y.-M. You, and R.-G. Xiong, Competitive halogen bond in the molecular ferroelectric with large piezoelectric response, J. Am. Chem. Soc. **140**, 3975 (2018).

[34] M. Kingsland, P. S. Ghosh, S. Lisenkov, and I. Ponomareva, Structural, electrical, and electromechanical properties of inverse hybrid perovskites from first-principles: The case of $(CH_3NH_3)_3OI$, J. Phys. Chem. C **125**, 8794 (2021).